BIOCHEMISTRY
including biophysical chemistry & molecular biology
Article

Biochemistry **XXXX,** *XXX,* 000–000 A
DOI: 10.1021/bi101307h

A Nuclear Magnetic Resonance-Based Structural Rationale for Contrasting Stoichiometry and Ligand Binding Site(s) in Fatty Acid-Binding Proteins†

Yan He,[‡,∥,§] Rima Estephan,[‡,∥] Xiaomin Yang,[‡,∥] Adriana Vela,[‡,∥] Hsin Wang,[‡,§,∥] Cédric Bernard,[§,∥] and Ruth E. Stark*[,‡,§,∥]

[‡]*Department of Chemistry, College of Staten Island,* [§]*Department of Chemistry, City College of New York, and* [∥]*City University of New York Graduate Center and Institute for Macromolecular Assemblies, New York, New York 10031, United States*

Received August 14, 2010; Revised Manuscript Received January 7, 2011

ABSTRACT: Liver fatty acid-binding protein (LFABP) is a 14 kDa cytosolic polypeptide, differing from other family members in the number of ligand binding sites, the diversity of bound ligands, and the transfer of fatty acid(s) to membranes primarily via aqueous diffusion rather than direct collisional interactions. Distinct two-dimensional $^{1}H-^{15}N$ nuclear magnetic resonance (NMR) signals indicative of slowly exchanging LFABP assemblies formed during stepwise ligand titration were exploited, without determining the protein−ligand complex structures, to yield the stoichiometries for the bound ligands, their locations within the protein binding cavity, the sequence of ligand occupation, and the corresponding protein structural accommodations. Chemical shifts were monitored for wild-type LFABP and an R122L/S124A mutant in which electrostatic interactions viewed as being essential to fatty acid binding were removed. For wild-type LFABP, the results compared favorably with the data for previous tertiary structures of oleate-bound wild-type LFABP in crystals and in solution: there are two oleates, one U-shaped ligand that positions the long hydrophobic chain deep within the cavity and another extended structure with the hydrophobic chain facing the cavity and the carboxylate group lying close to the protein surface. The NMR titration validated a prior hypothesis that the first oleate to enter the cavity occupies the internal protein site. In contrast, ^{1}H and ^{15}N chemical shift changes supported only one liganded oleate for R122L/S124A LFABP, at an intermediate location within the protein cavity. A rationale based on protein sequence and electrostatics was developed to explain the stoichiometry and binding site trends for LFABPs and to put these findings into context within the larger protein family.

Cytosolic fatty acid-binding proteins (FABPs) belong to a family from which more than 10 separate gene products have been identified and several classes of fatty acid transport functions have been proposed (*1*−*3*). These 14−15 kDa proteins are expressed abundantly in a tissue-specific manner that is essential to lipid metabolism; they have been isolated from mammalian tissues, including intestine, liver, heart, adipose tissue, myelin, brain, muscle, and epidermis, as well as from invertebrates such as locusts and hornworms (*4*). The FABPs have been found to enhance the transfer of long chain fatty acids (FAs)[1] between artificial and native lipid membranes in vitro and also to exert a stimulatory effect on a number of enzymes that control FA metabolism.

Though the amino acid sequence of rat liver FABP is only 22−27% homologous with those of FABPs from heart, adipose tissue, and myelin sheath, these latter proteins are 60−65% homologous to each other (*3*). Rat intestinal FABP has a sequence that is 29% homologous to that of liver FABP and also 30−33% homologous to those of the three proteins mentioned above. FABPs bind a variety of hydrophobic and amphipathic ligands with K_d values in the micromolar to nanomolar range. Although the divergent primary structures of the FABPs could account in principle for the different binding properties of the family members, their respective X-ray crystal structures exhibit an overall similarity, including a "clam-shell-like" configuration with two parallel β-sheets oriented orthogonally to each other and with the hydrophobic ligand(s) bound inside a cavity formed by the β-clam (*5*, *6*).

Liver-type fatty acid-binding protein (LFABP), which is expressed at millimolar levels in both intestinal absorptive cells and liver hepatocytes, is thought to play an essential role in dealing with increased levels of fatty acid flux that may occur in the enterocyte with high-fat diets or in the hepatocyte during starvation or uncontrolled diabetes. An important motivation for studying LFABP lies in its unique biochemical properties. First, LFABP binds diverse ligands relative to other FABPs. It can bind several FAs as well as endogenous hydrophobic ligands such as lysophospholipids, bile salts, and monoacylglycerols, whereas most other FABPs exhibit high-affinity binding to only FA (*2*, *7*). Second, LFABP possesses a very large hydrophobic binding cavity, which allows it to accommodate more than one FA

†This research was supported by grants from the National Institutes of Health (R01-DK38389), including a Minority Supplement to support the Ph.D. training of R.E., and by a Collaborative Research Grant (80209) from the City University of New York (CUNY). The NMR facilities used in this work are operated by The College of Staten Island, The City College, and the CUNY Institute for Macromolecular Assemblies, a Center of Excellence in Generating Employment through New York State Science program. Additional infrastructural support was provided at The City College of New York by National Institutes of Health Grant 5G12 RR03060 from the National Center for Research Resources.

*To whom correspondence should be addressed: CUNY Institute for Macromolecular Assemblies, The City College of New York, Department of Chemistry MR-1208B, 160 Convent Ave., New York, NY 10031-9101. E-mail: stark@sci.ccny.cuny.edu. Phone: (212) 650-8916. Fax: (212) 650-8719.

[1]Abbreviations: LFABP, rat liver fatty acid-binding protein; HSQC, heteronuclear single-quantum coherence spectroscopy; FA, long chain fatty acid; OLA, oleate; eq, molar equivalent.

ligand (*8*−*11*); other FABPs typically possess a single binding site for FA (*12*). Third, transport of anthroyloxyFA from LFABP to model membranes occurs more slowly than from intestinal, heart, or adipocyte family members and is controlled kinetically by aqueous diffusion of the fatty acid rather than being mediated by direct collisional interactions between the FABPs and the "acceptor" bilayer (*1*, *13*).

The high-resolution tertiary structure of LFABP in complex with oleic acid (oleate, OLA) has been determined independently by X-ray crystallography (*14*) and NMR spectroscopy (*8*); both reports indicate that wild-type LFABP binds two fatty acid molecules. One internally bound oleate molecule (OLA129) has a U-shaped conformation and lies deep within the cavity, inaccessible to solvent, whereas the other ligand (OLA128) adopts an extended conformation and is more exposed to the aqueous interface. It has been proposed that OLA129 enters the cavity first and presents a hydrophobic surface that can facilitate the subsequent binding of OLA128 (*14*), underscoring the putatively critical role of the first ligand binding step. Thus, in our NMR study of LFABP, we sought to monitor the progression of the ligand binding events at the molecular level, including the location of each FA with respect to particular protein sites and any attendant overall conformational changes that might reveal the basis for the anomalous binding properties of this protein family member.

Site-directed mutagenesis and chemical modification studies have implicated R122, S124, and S39 in the binding of OLA129 (*15*−*17*), which is likely to occur via direct electrostatic interactions with its carboxylate group and through hydrogen bonding networks mediated by water within the protein cavity (*14*, *18*). This rationale is supported by Multi-Conformational Continuum Electrostatics (MCCE) calculations (*19*, *20*) showing that R122 and S124 promote ionization of the OLA129 carboxylate, which then establishes favorable electrostatic interactions with a positively charged patch (R122, K125, and R126) on the inner surface of the cavity (*21*). To test how removing such interactions might affect the binding location, orientation, stoichiometry, and affinity of the protein−ligand complex, we replaced key positively charged and polar residues with nonpolar groups similar in size, e.g., by constructing an R122L/S124A double mutant of LFABP.

Whereas a detailed picture of the protein and its ligand(s) would emerge from determination of the tertiary structure of a protein−ligand complex by X-ray or NMR methods, it is desirable to obtain this information more rapidly and cost-effectively, particularly when a comparison of closely related macromolecular assemblies is desired. Although fluorescence (or isothermal titration calorimetry) measurements can provide the ligand stoichiometry and affinities (*22*), in practice the parameters for the second oleate bound to LFABP are sometimes challenging to determine (*21*); in any case, such methods do not reveal the molecular location(s) adopted by the ligands during the binding process. Amide ^{15}N NMR relaxation, ^{1}H exchange, and NMR line shape analyses such as those reported for apo- and holo-intestinal FABP, cellular retinol-binding protein, and bile acid-binding protein provide detailed conformational and motional information but focus exclusively on the protein rather than the protein−ligand complex(es) (*23*−*25*), whereas ^{13}C NMR relaxation of FABP-bound fatty acids reveals the dynamics and order of just the ligands (*26*).

^{15}N-edited heteronuclear single-quantum coherence (HSQC) NMR spectroscopy, which efficiently provides a two-dimensional map of amide HN chemical shifts for directly bonded groups in a protein, has been used extensively to study interactions between proteins and ligands in aqueous solution, for instance, to probe ligand binding sites (*27*, *28*), predict binding affinity (*29*), and elucidate structure−activity relationships relevant to drug discovery (*30*, *31*). Typically, chemical shift differences between free and bound protein are quantified by obtaining a weighted average of ^{1}HN and ^{15}N chemical shift perturbations (*32*). The perturbations arise from changes in the chemical environment of particular residues upon addition of ligand (e.g., involving hydrogen bonds, electrostatics, and hydrophobic interactions), revealing either a contiguous binding interface or more global protein conformational changes (*33*). In the studies presented here, stepwise addition of 0.4 molar aliquots of unlabeled oleate into ^{15}N-labeled wild-type and mutant LFABPs has been monitored using ^{15}N HSQC NMR spectra to determine the stoichiometry of the ligand(s) bound to each protein. Chemical shift resolution of NMR signals for the apo wild-type LFABP and its various OLA-liganded states also makes it possible to deduce the location and sequence of entry of each ligand into the protein cavity, confirming the 1:2 stoichiometry deduced from X-ray and NMR structures of the wild-type protein−ligand complex. A contrasting pattern of chemical shift perturbations is observed for oleate bound to R122L/S124A LFABP, supporting the binding of a single OLA ligand at a site intermediate between those occupied for the wild-type protein. The stoichiometry and ligand binding sites for these LFABPs, along with related family members, are examined in light of their respective protein sequences and electrostatic characteristics.

MATERIALS AND METHODS

Expression and Purification of Wild-Type and R122L/S124A [^{15}N]LFABP. The pET-11a vector containing either wild-type or R122L/S124A rat liver FABP cDNA was transformed into *Escherichia coli* host strain BL21(DE3) bacteria on agar plates containing 200 μg/mL ampicillin. After being rapidly grown in unlabeled rich medium to high cell densities (OD_{600} = 0.6), the transformed cells were harvested and then transferred into M9 minimal medium enriched with $^{15}NH_4Cl$ (Isotec, Miamisburg, OH), allowing subsequent growth to higher cell densities. After incubation for 1 h, protein expression was induced with 1.0 mM isopropyl β-D-1-thiogalactopyranoside (IPTG). The bacterial culture was incubated by being shaken at 225 rpm and 37 °C for 3 h. The cells were harvested and resuspended in Tris buffer (pH 8.3) and then purified chromatographically by size exclusion, ion exchange, and delipidation (*8*, *13*). Protein purity was confirmed by observation of a single band corresponding to a size of 14 kDa via sodium dodecyl sulfate−polyacrylamide gel electrophoresis. Typical yields of pure LFABP were 30 mg/L of bacterial culture.

Preparation of NMR Samples. Unlabeled sodium oleate was obtained from Sigma (St. Louis, MO), and the uniformly ^{15}N-enriched wild-type and R122L/S124A LFABP proteins were obtained as described above. A 100 mM stock solution of sodium oleate (pH 9.2) in H_2O was prepared to permit direct addition to each protein in phosphate buffer (pH 7.0) in a 5 mm NMR tube. For ^{15}N HSQC titration of wild-type LFABP, 1.8 μL aliquots of 100 mM oleate were added to 579 μL of 0.783 mM apoprotein in phosphate buffer (50 mM Na_2HPO_4/NaH_2PO_4, 100 mM NaCl, 5 μM EDTA, and 0.02% NaN_3), corresponding to increments of 0.4 molar equivalents (eq) oleate added successively to the

protein. A total of six complexes of ^{15}N-labeled wild-type LFABP with oleate at ratios of 1:0.4, 1:0.8, 1:1.2, 1:1.6, 1:2.0, and 1:3.0 were prepared for the NMR titration experiments. For ^{15}N HSQC titration of R122L/S124A LFABP, 2.0 μL aliquots of 100 mM oleate were added to 550 μL of 0.906 mM apoprotein in phosphate buffer (50 mM Na_2HPO_4/NaH_2PO_4, 100 mM KCl, 5 μM EDTA, and 0.02% NaN_3), each representing the addition of 0.4 eq of oleate to the protein. A total of five complexes of ^{15}N-labeled R122L/S124A LFABP with oleate at ratios of 1:0.4, 1:0.8, 1:1.2, 1:2.0, and 1:3.0 were prepared for the collection of NMR titration data. No changes in solution pH were observed after addition of successive aliquots of oleate.

^{15}N HSQC NMR Experiments and Data Analysis. ^{15}N HSQC NMR experiments (*34*) were conducted on a four-channel Varian ^{UNITY}INOVA 600 MHz spectrometer, with observations made at 10 °C to optimize spectral resolution and avoid multiple conformations of the unliganded protein. The H_2O signal (4.91 ppm) was set on resonance in the proton dimension, and the ^{15}N carrier was set in the middle of the amide region (120.54 ppm). Chemical shifts were referenced following the guidelines of Wishart and Sykes (*35*). The experiments were conducted with 256 complex points in t_1, 1024 complex points in t_2, and 32 transients. The NMR spectra were processed with NMRPipe (*36*) and analyzed using NMRView (*37*). Chemical shift perturbations for each backbone HN cross-peak were calculated, for instance, as follows: $\Delta(\text{apo}-\text{sgl}) = ([\delta_{HN}(\text{apo}) - \delta_{HN}(\text{sgl})]^2 + \{[\delta_N(\text{apo}) - \delta_N(\text{sgl})]/6.5\}^2)^{1/2}$ (*32*), where sgl refers to the singly liganded protein.

Backbone HN Resonance Assignments for Wild-Type LFABP Titration. ^{1}H$-^{15}$N HSQC spectra were recorded at each step of the titration of unlabeled oleate into ^{15}N-labeled wild-type LFABP. As described previously (*8*), a single set of backbone HN peaks was observed for both apo-LFABP (without any bound ligand) and holo-LFABP (with 2 eq of bound oleate). The backbone HN resonance assignments for each of these forms were derived from our previous reports (*8*, *38*); minor peak shifts were attributed to different choices of pH or temperature but did not complicate the analysis. At the 0.4 eq titration stage, the backbone HN signals attributed to a singly liganded variant of the protein (sgl-LFABP) were assigned by visual comparison with the HSQC spectrum of apo-LFABP and confirmed by correlation to both backbone and side chain ^{1}H and ^{13}C nuclei using a set of three-dimensional coherence transfer NMR data sets obtained from uniformly ^{15}N- and ^{13}C-labeled LFABP titrated with 0.4 eq of oleate (data not shown). At other titration stages, the HN assignments were completed by tracking the chemical shift changes visually but unambiguously. Considering all forms of each protein, the completeness of the backbone HN assignments was 98.2% for the wild-type protein.

Backbone HN Resonance Assignments for R122L/S124A LFABP Titration. Sequential assignments of ^{1}H, ^{15}N, and ^{13}C nuclei in apo- and holo-R122L/S124A LFABP were made by standard through-bond correlation procedures (*38*), including a set of multidimensional NMR experiments performed on a uniformly ^{15}N- and ^{13}C-labeled protein (*21*). The backbone HN assignments at titration stages of 1:0.4, 1:0.8, and 1:1.2 were completed by comparison of the HN peak positions to both apo and 1:2.0 proteins and by recognition of the peak patterns for preceding or subsequent titration steps. Four residues (G37, M74, G106, and D107) had either missing or ambiguous HN shifts, resulting in 96.0% completeness of the backbone HN assignments for the R122L/S124A LFABP titration.

RESULTS

Observation of Intermediate Oleate-Bound States for Wild-Type LFABP. Standard chemical shift perturbation methods were extended to map site-specific changes in the protein magnetic environment at each stage of the titration with a fatty acid ligand. For wild-type LFABP, stepwise titration monitored through the protein HN resonances in two-dimensional (2D) NMR spectra revealed intermediate binding states in addition to the apo and doubly liganded (holo) forms. Moreover, well-resolved backbone resonances that could be attributed to complexes designated as apo, sgl, and holo were found to coexist in slow exchange on the NMR time scale, suggesting the possibility of using ^{1}H$-^{15}$N HSQC to deduce both the location of each OLA molecule that enters the protein cavity and the stoichiometry of ligand binding.

Figure 1 illustrates protein ^{1}H$-^{15}$N HSQC spectra recorded at various titration points (apo, 1:0.4, 1:0.8, 1:1.2, 1:1.6, and holo (1:2)), displaying several notable spectral features at each stage. (1) Two sets of HN signals were observed when the first 0.4 eq of oleate was added to LFABP, one set from apo-LFABP and the other from sgl-LFABP. The intensities of the two sets of signals were roughly equivalent at this early titration stage, indicating a preference for the liganded state and consistent with K_d estimates of 9−40 nM (*21*, *22*). The composite chemical shift difference between the apo- and sgl-LFABP signals varied significantly along the protein sequence, from 0.002 to 0.850 ppm (*32*). (2) With the addition of the second 0.4 eq of oleate to LFABP, that is, cumulatively 0.8 eq, the HN signals from apo-LFABP were either absent or greatly diminished; the HN peaks from sgl-LFABP were retained with slightly increased intensities, and a new set of HN resonances appeared with intensities weaker than those of sgl-LFABP but chemical shifts identical or nearly identical to those of holo-LFABP, thus designated herein as preholo-LFABP. The chemical shift difference between the sgl- and preholo-LFABP resonances also varied significantly along the polypeptide chain, from 0.002 to 1.36 ppm. (3) The HN resonances from sgl and preholo forms of LFABP were retained at their respective positions upon addition of 1.2 eq of oleate, but the relative intensities of these slowly exchanging sets of signals were reversed. (4) When the amount of titrated ligand reached 1.6 eq, only one set of HN resonances was observed, which can be attributed to holo-LFABP. (5) At 2.0 eq, the HN resonances from holo-LFABP exhibited the same spectral features as those with 1.6 eq. The chemical shift difference between preholo-LFABP and holo-LFABP forms was typically modest, with 78% of the residues shifted less than 0.02 ppm and only two residues varying by more than 0.05 ppm (0.075 ppm for K96 and 0.085 ppm for F95); these latter protein forms exhibited rapid chemical exchange and thus population-averaged NMR signals. The holo-LFABP designation corresponds to prior crystallographic and NMR determinations of two bound oleate ligands (*8*, *14*). (6) Finally, at 3.0 eq, the HN peaks were sharpened further, but the resonance positions remained essentially the same as those at 2.0 eq, indicating that two ligands remained bound to the protein and the excess ligand was presumably free in solution.

In summary, four unique sets of HN resonances were observed for the protein during the titration process, corresponding to distinct apo-, sgl-, preholo-, and holo-LFABP structural forms. In addition to the commonly identified apo form with no ligands and the fully bound holo form with two oleate ligands, it was possible to characterize structural species at intermediate sgl and

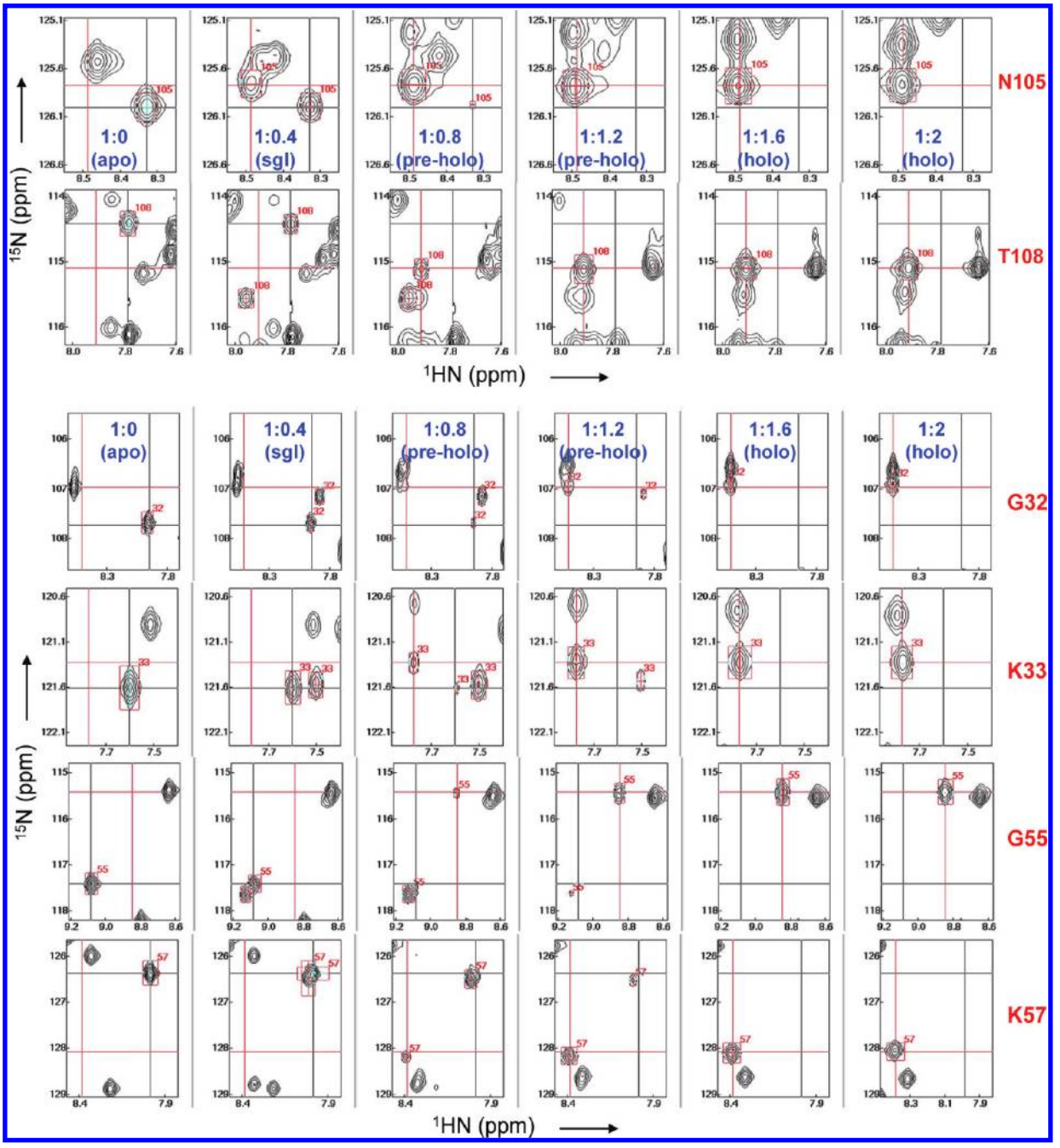

FIGURE 1: Expanded regions of $^{1}H-^{15}N$ HSQC contour plots for selected wild-type LFABP residues upon titration with oleate ligands up to a protein:ligand ratio of 1:2.0. Chemical shifts are referenced according to the guidelines of Wishart and Sykes (*35*). NMRView is used to illustrate chemical shift changes between the apo peaks centered at the black cursor, the holo peaks centered at the red cursor, and other labeled peaks corresponding to various titration stages. The top panels illustrate amino acid residues with Δ(apo−sgl) being larger than Δ(sgl−holo), whereas the bottom panels show examples for which Δ(sgl−holo) is larger than Δ(apo−sgl).

preholo stages of the binding process. As detailed below, the HN resonance assignments of sgl-LFABP are critical for understanding the binding stoichiometry and protein−ligand interactions because they reveal significant site-specific variations with respect to either apo-LFABP (0.002−0.85 ppm) or holo-LFABP (0.002−1.32 ppm). The stepwise ^{15}N HSQC titration analysis of wild-type LFABP is summarized by HN assignments tabulated for apo-, sgl-, preholo-, and holo-LFABP at 10 °C and pH 7.0 (Table S1 of the Supporting Information), and plots of chemical shift perturbation along the protein sequence (Figure 2A).

Stoichiometry and Entry of Oleates Bound to Wild-Type LFABP. Although the presence of two oleates at distinct LFABP binding sites has been demonstrated from X-ray and NMR structures determined for the holoprotein complex (*8*, *14*) and through our ^{13}C HSQC NMR study of ligand exchange phenomena (*18*), our current strategy exploits the observation of resolved signals for apo-, sgl-, preholo-, and holo-LFABP in ^{15}N HSQC spectra to deduce the stoichiometry of OLA bound to LFABP independently and exclusively from ^{15}N chemical shift perturbation analysis of the protein resonances.

As shown in Figures 2A and 3A, there are 30 amino acid residues with magnitudes of the chemical shift difference Δ(apo−sgl) above a threshold of 0.15 ppm, 21 of which show Δ(apo−sgl) > Δ(sgl−holo) and, thus, the bulk of the environmental change occurring upon binding of the first ligand. The quantity Δ(apo−sgl) exceeds Δ(sgl−holo) by more than 0.15 ppm for

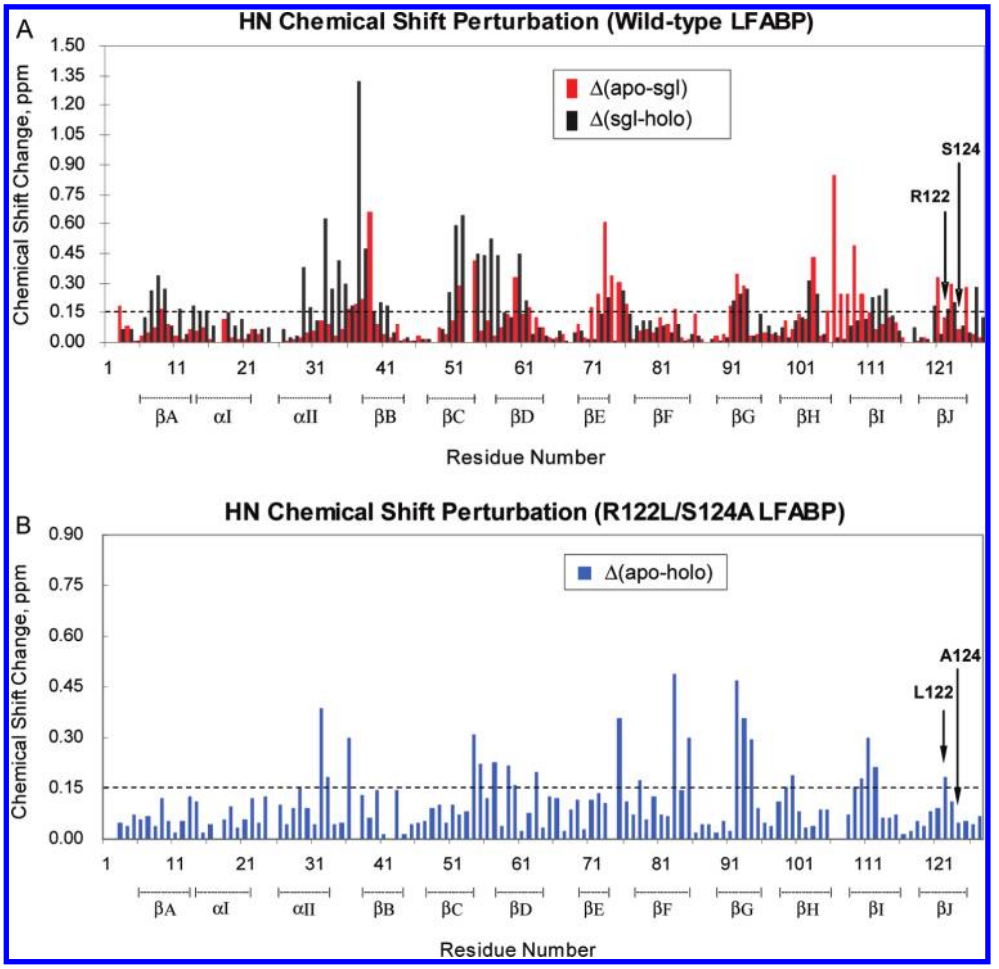

FIGURE 2: Composite $^{1}H-^{15}N$ chemical shift perturbation plotted along the protein sequence and with respect to secondary structural elements for (A) wild-type LFABP and (B) R122L/S124A LFABP. Note that the *y*-axes differ for wild-type and double mutant proteins, with average perturbations nearly twice as large for wild-type LFABP. The apo, sgl, and holo notations refer to protein:ligand molar ratios of 1:0, 1:0.4, and 1:2.0, respectively. Chemical shift perturbations are calculated, for instance, as $\Delta(\text{apo}-\text{sgl}) = ([\delta_{HN}(\text{apo}) - \delta_{HN}(\text{sgl})]^2 + \{[\delta_N(\text{apo}) - \delta_N(\text{sgl})]/6.5\}^2)^{1/2}$ (*32*). The dashed lines at 0.15 ppm, set slightly below the mean ± the standard deviation for each pair of protein forms, serve as a guide for identifying backbone sites with structurally significant chemical shift changes.

11 of those backbone sites: S39, L71, T73, E103, N105, G106, D107, T108, I109, K121, and K125. Thus, we consider provisionally that these 11 spatially proximal residues comprise the binding site for the first ligand and the corresponding ligand binding environment of the sgl-LFABP protein structure. By mapping these amino acids onto the NMR structure of the oleate-bound LFABP (Figure 3B, highlighted in red) [Protein Data Bank (PDB) entry 2ju8 (*8*)], we find their clustered location near particular β-strands (βB, βE, βI, and βJ) and a $\beta-\beta$ loop (βH$-\beta$I turn) becomes evident, validating our interpretation in terms of ligand location rather than overall protein structural rearrangements. Notably, no residues in the helical regions show any significant chemical shift perturbations when the apo and sgl proteins are compared.

Conversely, there are 41 residues with Δ(sgl−holo) values of >0.15 ppm (Figures 2A and 3A), 34 for which Δ(sgl−holo) > Δ(apo−sgl) and 20 for which Δ(sgl−holo) exceeds Δ(apo−sgl) by more than 0.15 ppm: Y7, Q8, I29, G32, K33, D34, I35, G37, V38, L50, T51, I52, G55, S56, K57, T102, T112, M113, Y120, and R126. The significant Δ(sgl−holo) magnitudes indicate that these latter residues are involved in additional ligand binding; a sequential model for transformation of the protein structure from sgl-LFABP to holo-LFABP is proposed below. Figure 3B highlights these sites in green and demonstrates that these latter amino acids are located not only in particular β-strands (βC, βI, βJ, and βC$-\beta$D turn) but also in the helical region (αII and αII$-\beta$B turn) of the protein structure. Therefore, besides the primary binding site, a second binding locus of the oleate in wild-type LFABP exists, associated with significant chemical shift perturbations from sgl- to holo-LFABP, either directly by entry of the ligand into the cavity or via repositioning of the first fatty acid.

Given the space available within the protein cavity and the length of the long chain oleate molecule (Figure 3C), the NMR titration data described above also provide evidence that the ratio of wild-type holo-LFABP to oleate is 1:2. The chemical shift perturbations observed between apo- and sgl-LFABP confirm that the first oleate molecule resides internally spanning opposite sides of the β-barrel structure (ends of the ligand at the βE$-\beta$F and βH$-\beta$I turns), consistent with the location of OLA129 reported in the solution- and solid-state structures of the holo-LFABP complex (*8*, *14*). Further titration of the sgl-LFABP form to preholo- or holo-LFABP demonstrates that the second oleate molecule has an extended conformation near the surface of the protein (near αII and the βC$-\beta$D turn), again in accord with the location of OLA128 reported for the ligand−protein complex. These NMR titration experiments suggest that the interior binding site is occupied first by OLA129 and the surface-accessible site is filled subsequently by OLA128, but

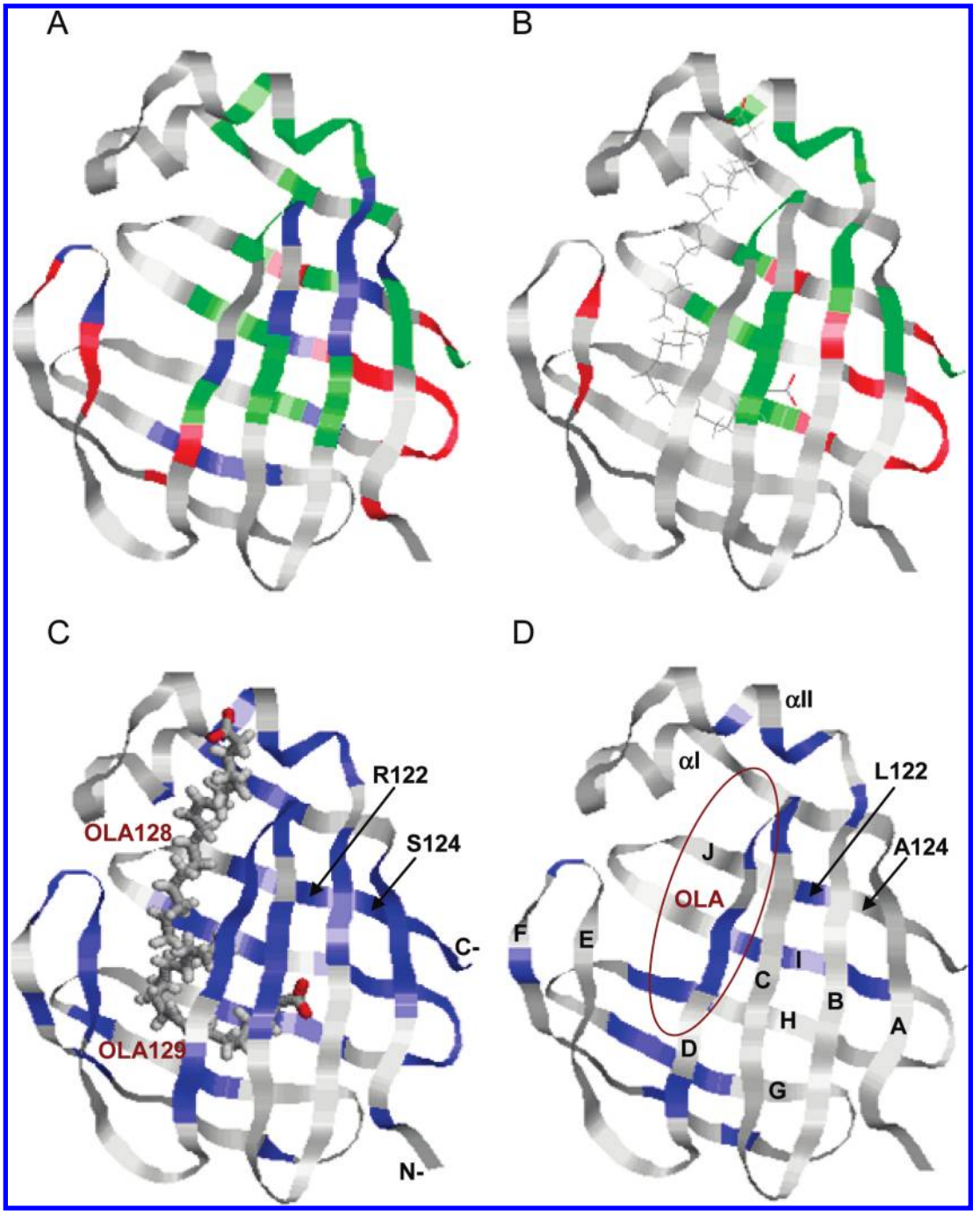

FIGURE 3: Structural view using Rasmol (http://www.RasMol.org) for HN chemical shift perturbations of oleate titrated into wild-type LFABP (A−C) and R122L/S124A LFABP (D) [PDB entry 2ju8 for the protein−ligand complex (*8*, *21*)]. Residues are highlighted in terms of the degree of chemical shift perturbation upon ligand binding. In panel A, residues are colored red when Δ(apo−sgl) > 0.15 ppm, green when Δ(sgl−holo) > 0.15 ppm, and blue when both Δ(apo−sgl) and Δ(sgl−holo) exceed 0.15 ppm. Panel B compares the impact of binding of the first and second ligands to wild-type LFABP: red when Δ(apo−sgl) exceeds Δ(sgl−holo) by 0.15 ppm so the effect of the first ligand predominates and green when Δ(sgl−holo) exceeds Δ(apo−sgl) by 0.15 ppm so the effect of the second ligand predominates. In panel C, residues are colored blue if Δ(apo−holo) > 0.15 ppm when both oleates bind to wild-type LFABP, and this structure shows the ligand locations derived from NMR measurements (*8*). In panel D, residues are colored blue if Δ(apo−holo) > 0.15 ppm when oleate binds to R122L/S124A LFABP, showing the deduced binding region for the sole ligand circled in brown. Additional explanations appear in the text.

alternative sequential and parallel binding models are considered below.

Chemical Shift Perturbation and Oleate-Bound States upon Stepwise Titration of R122L/S124A LFABP. Figure 4 displays R122L/S124A LFABP $^{1}H-^{15}N$ HSQC spectra observed at several titration points: apo, 1:0.4, 1:0.8, 1:1.2, and 1:2. Chemical shift index analysis (*35*) showed essentially identical secondary structural elements for both apo and holo forms of the double mutant as compared with the wild-type proteins, arguing against reorganization of the LFABP tertiary structure (*21*) and in accord with the overall structural similarity of family members that possess a relatively modest degree of sequence homology (*4*, *10*, *21*, *39*). A single set of backbone HN peaks was evident for each of the apo and holo forms of the double mutant protein, but as for wild-type LFABP, the 1:0.4 titration stage displayed distinct HN signals (in this case with a similar integrated

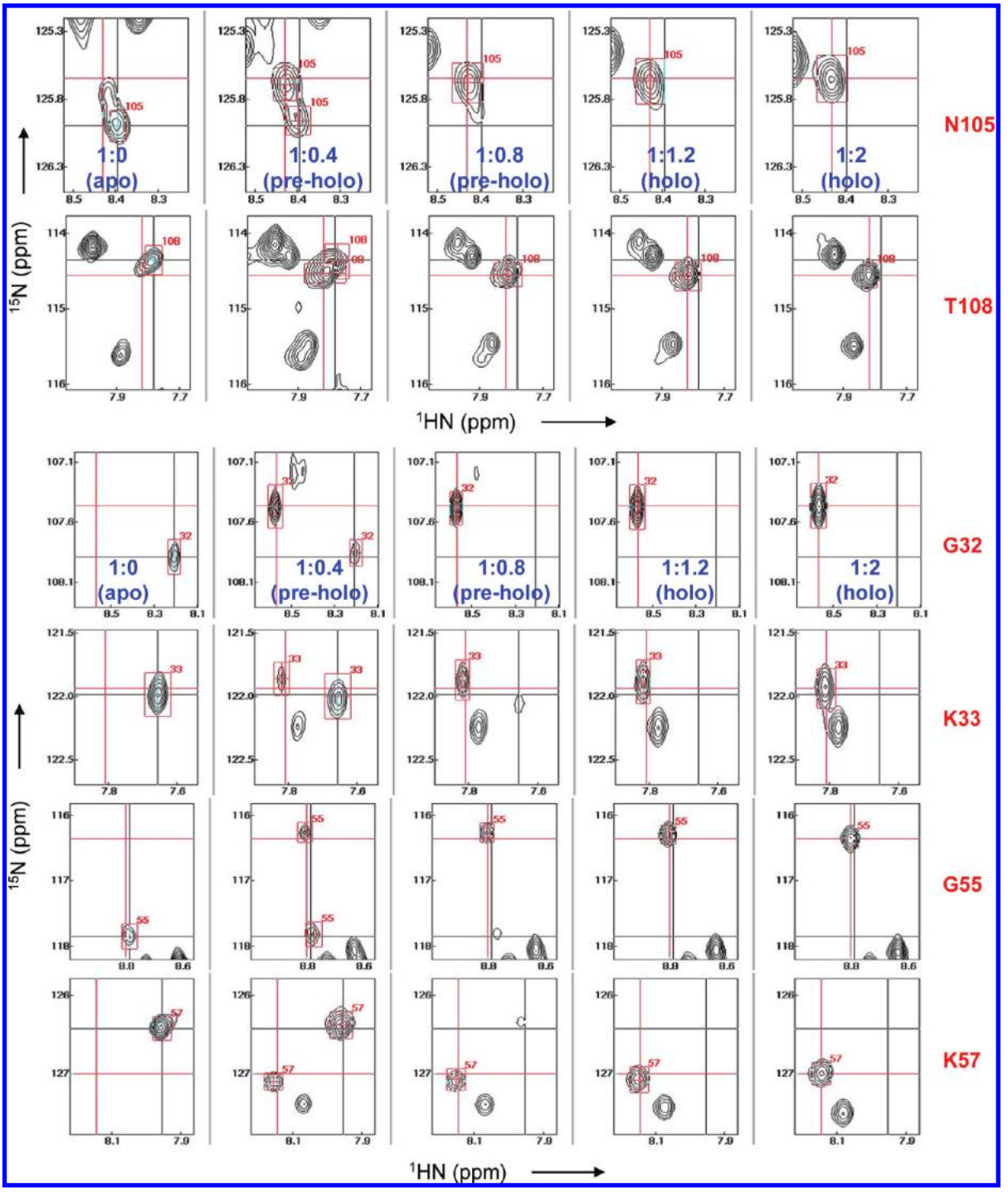

FIGURE 4: Expanded regions of $^{1}H-^{15}N$ HSQC contour plots for R122L/S124A LFABP upon titration with oleate, highlighting the same residues shown in Figure 1 for the wild-type protein. Chemical shifts are referenced according to the guidelines of Wishart and Sykes (*35*). NMRView is used to visualize the apo peaks centered at the black cursor and the 1:2 holo peaks centered at the red cursor. Very modest chemical shift perturbations were observed for titration beyond a protein:oleate molar ratio of 1:0.4.

intensity) for both apo and liganded proteins. The chemical shift difference between the two sets of signals varied along the protein sequence, from 0.002 to 0.523 ppm (Figure 2B). The average value of Δ(apo−holo) for the backbone residues of R122L/S124A LFABP was 0.107 ppm, approximately half the magnitude observed in the wild-type protein for Δ(apo−holo) and similar to its value of Δ(apo−sgl). The apo peaks disappeared at and beyond a ratio of 1:0.8, confirming the expected predominance of the liganded form at our concentration of 900 μM, given the 450 nM K_d estimated for the first binding event (*21*). For oleate titrated into the R122L/S124A protein, we designate the 0.4 and 0.8 eq complexes as preholo-R122L/S124A and the titration points of ≥1.2 eq as holo-R122L/S124A. The preholo resonances exhibited very modest changes in chemical shift at the remaining titration steps up to 3.0 eq (maximum variation of 0.06 ppm), but such changes in shift, intensity, and/or line width support the presence of two (or more) rapidly exchanging liganded states discussed below. Thus, the oleate−protein binding process differs fundamentally for an R122L/S124A LFABP mutant in which we have removed electrostatic interactions viewed as essential to fatty acid binding: it lacks the slowly exchanging sgl-LFABP stage seen for the wild-type protein and exhibits only

two major sets of HN resonances in the ^{15}N HSQC NMR spectra. The stepwise ^{15}N HSQC titration analysis of R122L/S124A LFABP includes HN assignments tabulated at 10 °C and pH 7.0 (Table S2 of the Supporting Information) and plots of chemical shift perturbation along the protein sequence (Figure 2B).

Stoichiometry and Location of Oleate Bound to R122L/S124A LFABP. The observation of just two sets of ^{15}N HSQC signals, coupled with an average Δ(apo−holo) that is half the magnitude of that of wild-type LFABP and the failure to observe chemical shift perturbations at any additional sites for titration points beyond 0.4 eq of added ligand, suggests that the stoichiometry is 1:1 for the mutant protein−OLA complex. The observed pattern of protein spectral changes is also in accord with observations of the ligand in NMR titration experiments, for which addition of 2 eq of uniformly ^{13}C-labeled oleate produces two sets of ^{1}H and ^{13}C resonances in ^{13}C HSQC for wild-type LFABP (*18*) but only one such set for the mutant protein (*21*). Possible interpretations of small chemical shift changes observed at later stages of the titration are discussed below.

As shown in Figure 2B, 24 polypeptide residues exhibit an HN chemical shift difference (between apo- and holo-R122L/S124A LFABP) of >0.15 ppm: I29, G32, K33, K36, Y54, G55, K57, I59, H60, F63, T75, K78, V83, M85, V92, T93, T94, K99, S100, I109, T110, N111, T112, and L122. Because the holo structures are quite similar for wild-type and R122L/S124A LFABP (*8*, *21*), highlighting the perturbed residues on the wild-type protein solution structure made it possible to compare the ligand binding sites of the two proteins (Figure 3D). T75, I109, N111, T110, and L122 are situated close to the first oleate binding site of wild-type LFABP, whereas I29, G32, K33, K36, Y54, G55, K57, I59, H60, K99, S100, and T112 are close to the second oleate binding site of the wild-type protein. Five additional perturbed residues, V83, M85, V92, T93, and T94, which are located along strands βF and βG, define a binding region for oleate that is unique to the mutant protein. As a group, 22 of 24 perturbed residues (excluding F63 and K78) comprise a localized binding region that supports the presence of a single OLA molecule in the binding cavity of R122L/S124A LFABP and allows us to deduce with reasonable certainty the location and conformation of this bound ligand. As designated by the brown oval in Figure 3D, we propose that the oleate ligand is bound to the mutant protein in an extended conformation, with its carboxylate head pointing toward the helical region (near K33 or K36) and its methyl tail close to the hydrophobic amino acids, V83 and/or V92. Docking calculations with chemical shift perturbation and intermolecular NOE restraints are in progress to test this hypothesis. Comparisons with wild-type LFABP, other members of this protein family, and an electrostatic rationale for these trends are outlined below.

DISCUSSION

Chemical Shift Mapping versus Structure of the Wild-Type LFABP−Oleate Complex. As demonstrated above, monitoring the protein ^{15}N HSQC spectra during stepwise ligand titration allowed for an independent determination of the 1:2 wild-type LFABP:OLA stoichiometry deduced previously by full structure determinations of the complex (*8*, *14*). Moreover, the observation of an intermediate sgl-LFABP liganded structure allowed us to discriminate between the internal and surface-exposed binding sites that are occupied by OLA molecules within the protein cavity.

An internal binding site for the first oleate was proposed to include the following residues: S39, L71, T73, E103, N105, G106, D107, T108, I109, K121, and K125. Although a structure for the singly liganded complex has not yet been reported, it is possible to evaluate this proposal by reference to the amino acid residues located proximally with respect to the internal OLA129 ligand in the reported structures of holo-LFABP (*8*, *14*). For example, S39, R122, and S124 are involved in hydrogen bonding interactions with the carboxyl group of OLA129 in holo-LFABP crystals (*40*); residues near the turns βH and βI (N105, G106, D107, T108, and I109) are spatially close to only the primary OLA129 ligand (*8*, *14*); I41, E72, T73, and T102 are recognized as packing closely with OLA129 in conjunction with entropically favorable displacement of ordered water molecules from the rat LFABP protein cavity (*40*); and intermolecular nuclear Overhauser effects (NOEs) are observed by solution NMR between proton pairs of OLA129 with I41, L71, and I109 (*8*). Thus, these comparisons of sgl- and holo-LFABP suggest that many segments of the first oleate reach their final locations within the protein cavity upon initial entry and do not contribute to the chemical shift changes measured subsequently as Δ(sgl−holo).

Analogously, a binding site for the surface-accessible oleate was proposed to involve amino acids closer to the aqueous interface: Y7, Q8, I29, G32, K33, D34, I35, G37, V38, L50, T51, I52, G55, S56, K57, T102, T112, M113, Y120, and R126. Among the residues listed above and their neighbors, K31, Y54, and S56 are involved in the hydrogen bonding network of OLA128 (*38*); several side chain atoms of the predominantly nonpolar residues L28, G32, I35, I52, Y54, G55, and M113 are in contact with the hydrophobic chain of that ligand (*40*); and intermolecular NOEs are observed between OLA128 and L28, G32, I35, G37, I52, Y54, K57, I59, and Y120.

Taken together, these results demonstrate the usefulness of extending the well-established chemical shift mapping method for the identification of protein−ligand binding sites to delineate the binding events that occur when multiple ligands are bound to a protein target, provided that the various forms are resolved spectroscopically. Such analyses of NMR chemical shifts or line shapes can be useful, for instance, for gaining molecular insights into allosteric regulation of protein function (*25*). Chemical shift mapping of environmental perturbations for a protein may also complement the assessments of binding energetics derived from isothermal titration calorimetry or NMR of the ligands, as demonstrated in the human ileal bile acid binding protein multisite system (*41*).

For doubly liganded wild-type LFABP, both sequential and parallel stepwise binding models may be considered (*25*, *41*). The latter model would require formation of a protein complex with a single oleate bound at one site as well as a complex with a single oleate bound at the other site. Tight binding of FA ($K_d \sim 9-60$ nM) has been reported at both sites (*22*). Thus, if binding were to occur in a parallel fashion at both of these sites, the rate of exchange between the two singly liganded complexes would likely be too slow to average the NMR signals, and we should observe distinct HSQC cross-peaks. No such peaks were observed for any protein backbone residues, though the smaller population of the more weakly liganded state could make it challenging to detect in the NMR spectrum. In addition, the X-ray structure of doubly liganded LFABP shows that the protein has only one contiguous cavity instead of two distinct binding pockets (*14*), making it difficult to envision the existence of a complex that is singly liganded at a much weaker site. Finally, upon titration of LFABP

with [U-^{13}C]oleate, we previously observed an α-methylene ^{1}H resonance at 1.89 ppm that appeared initially, and two resonances at 1.72 and 2.22 ppm at the end point of the titration (*18*). Both of the upfield resonances (1.72 and 1.89 ppm) have shifts quite different from those of bulk oleate; they may be attributed to a methylene group next to a carboxylate that is salt-bridged with a basic residue. Taken together, these observations support a sequential model in which the first FA molecule binds at the interior wild-type LFABP site via a salt bridge tether to R122 and the second oleate binds at an aqueous-accessible portal protein site. Chemical shift variations observed for both ligand and protein resonances at the later titration stages may reflect environmental changes for the protein, the ligand, or both partners.

Accommodation of the Two Oleate Ligands within the Wild-Type LFABP Binding Cavity. An intermediate state designated as preholo-LFABP was observed at titration stages between 0.8 and 1.2 eq of oleate, suggesting an "accommodation" of the sgl protein to the entry of the second oleate ligand (OLA128) into the protein cavity. The preholo and holo states exhibit small chemical shift differences (<0.02 ppm for 78% of the residues) but undergo exchange averaging rather than displaying separate resonances, a reasonable result in light of the weaker binding reported for the second ligand (*21*, *22*, *42*). Among the 2% of residues that have HN shift differences exceeding 0.05 ppm between preholo- and holo-LFABP, F95 (0.085 ppm) and K96 (0.075 ppm) are located near the βG−βH turn and close to the first oleate ligand, although they do not exhibit significant values of Δ(apo−sgl). Such shift changes could reflect adjustments of the OLA129 segments proximal to F95 and K96 that occur only upon entry of the OLA128 ligand into the protein cavity. In contrast, G32, G37, and Y54 exhibit substantial values of both Δ(sgl−holo) (≥0.50 ppm) and Δ(preholo−holo) (∼0.04 ppm) as well as intermolecular NOEs with OLA128. Together, these observations suggest that these latter residues are not only contributing directly to binding of the second OLA128 ligand but also experiencing the effects of "resettling" by the first OLA129 ligand, after both fatty acids have entered the binding cavity. The observation of small protein chemical shift perturbations as the second fatty acid binding site becomes occupied is also in accord with the hydrophobic interactions that have been postulated to occur between OLA128 and OLA129 (*38*) and thought to be enhanced by a swiveling of the polar K90 side chain outward toward the aqueous solvent (*8*). As we will discuss below, this capacity for subtle accommodation of the LFABP protein structure to adjust the electrostatic character of the binding cavity may be a key prerequisite for recruitment of diverse or multiple ligands.

Molecular Environment and Orientation of the Oleate Bound to R122L/S124A LFABP. Unlike doubly liganded wild-type LFABP, R122L/S124A LFABP has a binding region defined by residues I29, G32, K33, K36, Y54, G55, K57, I59, H60, T75, V83, M85, V92, T93, T94, K99, S100, I109, T110, N111, T112, and L122, as judged by stepwise ^{15}N HSQC NMR titration. A likely oleate orientation and conformation may also be proposed: the carboxyl group will point toward K33 or K36 because a hydrogen bond can form between the ligand COO group and the side chain NH_3 group of the lysine residue. The hydrocarbon tail of the oleate could then approach V83 and V92, promoting hydrophobic interactions between the protein and the ligand. In this scenario, the bound oleate would adopt an extended conformation within the R122L/S124A LFABP cavity, spanning strands βJ to βF in a way that perturbs chemical shifts of the residues listed above. The rather modest degree of conformational adjustment evidenced by chemical shift and intensity changes beyond the addition of 0.4 eq of oleate ligand is also a reasonable result if only a single fatty acid binds to the protein.

Stoichiometry and Electrostatics of Oleate Binding to LFABPs. Though the solution structures of wild-type and R122L/S124A LFABP are similar (*21*), our NMR titration results suggest that the mutant binds a single oleate; only the wild-type protein is able to accommodate two fatty acid molecules. Slowly exchanging apoprotein, single-liganded protein, and holoprotein resonances are evident for wild-type LFABP, which also displays separate ligand resonances in the doubly liganded state (*18*). For the double mutant, no distinct NMR signals are observed for multiple liganded states or multiple fatty acid ligands (*21*). Nonetheless, modest changes in chemical shift observed at the later titration stages support the presence of two (or more) rapidly exchanging liganded states for R122L/S124A LFABP. If the late-appearing state were a doubly liganded protein, the progressively changing shifts would indicate weak binding ($K_d \geq 1$ mM) and the second ligand would be expected to perturb a host of additional protein backbone sites. A more likely explanation for the late-stage spectral changes invokes conformational accommodation of a singly liganded protein: (a) the total shift perturbation is only half as large as for doubly liganded wild-type (wt) LFABP (Figure 2); (b) titration beyond the 1:0.4 stage results in no additional perturbed sites and maintains a smaller locus of affected residues than for wt-LFABP (Figure 3); (c) conformational accommodation is plausible because the chemical shift changes occur at protein sites near the portal region, which often displays greater flexibility in FABPs and where oleate is estimated to bind 6 times less tightly in wt-LFABP (*21*, *22*).

Examination of the electrostatic potential surfaces for both apoproteins provides a rationale for the entry of oleate molecule(s) into the respective LFABP cavities. As noted previously (*8*), the inner surface of the wild-type apo-LFABP cavity is studded with positively charged K90 and R122 groups (Figure 5A). K90, with a positive charge located deep within the binding cavity (near the flexible βF−βG turn), may be able to recruit the first OLA129 ligand. The structure of the wild-type oleate-bound complex (*8*, *14*) provides evidence of a hydrogen bond between the carboxyl oxygen of the internal ligand OLA129 and the side chain NH_2 proton of R122 that could play a key role in establishing the first ligand binding site. If, as we hypothesized previously (*8*), the K90 side chain then swivels outward, it would be possible to create a less crowded and more hydrophobic local environment for the second OLA128 ligand (Figure 5B). For the latter oleate, an extended conformation is favored by electrostatic interactions between the carboxyl group and K31, as well as by hydrophobic interactions with the ω-methyl group and the OLA129 chain.

Not surprisingly, formation of the key hydrogen bond is precluded for a mutant LFABP in which R122 and nearby S124 residues are both replaced with hydrophobic residues of similar size. As noted above, Multi-Conformational Continuum Electrostatics (MCCE) calculations (*19*, *20*) also indicate that R122 and S124 promote ionization of the OLA129 carboxyl group, so in the absence of these residues, both electrostatic attraction and hydrogen bonding between protein and ligand could well be compromised. Thus, the oleate molecule is not likely to reside deep within the R122L/S124A β-clam pocket, and

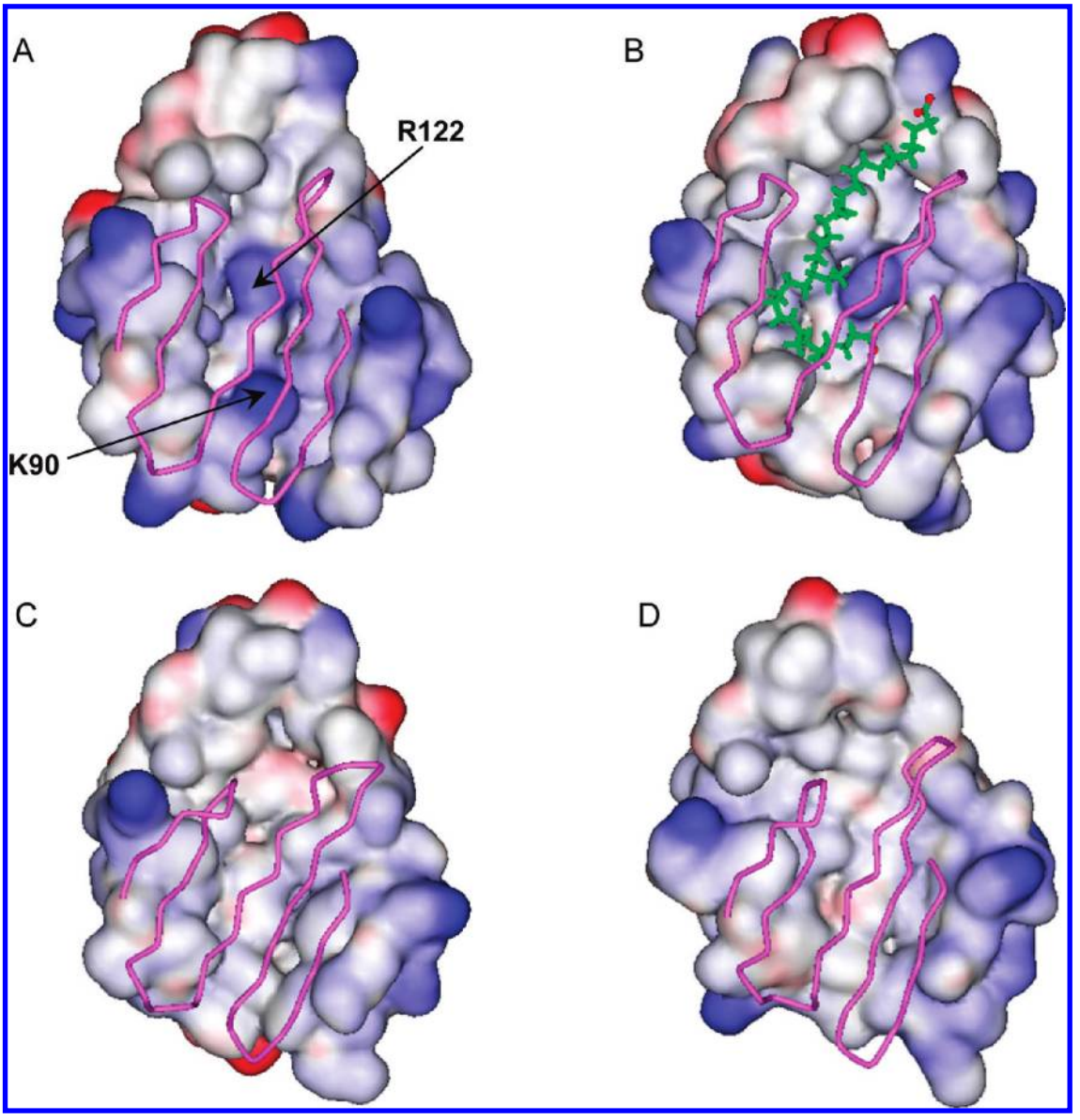

FIGURE 5: Electrostatic potential surface views inside the cavities of wild-type apo-LFABP and the OLA−LFABP complex [A and B (*8*)] and for apo- and holo-R122L/S124A LFABP [C and D (*21*)], displayed with DS ViewerPro. Calculations were performed at pH 7 assuming that the Asp, Glu, Arg, and Lys residues are ionized (*43*). The inner protein surfaces are displayed for residues 1−37 and 81−127. Surface charges are colored blue (positive), red (negative), and white (neutral). Protein backbone traces of β-strand residues 38−80 are colored pink; ligands are colored green. K90 is not visible in panels B−D because its side chain faces the outer surface of the protein.

presumably, no hydrophobic surface is formed within the protein cavity to promote binding of a second ligand.

Moreover, the K90 side chain of the double mutant apoprotein faces outward from the surface (Figure 5C) (*21*), as in wild-type holo-LFABP and as previously reported for analogous residues in ILBP, CRABP(II), and IFABP (*44*−*46*). Because the R122L and S124A mutations are likely to create a more hydrophobic environment within the cavity compared with that of wild-type LFABP, swiveling of the positively charged K90 side chain outward toward the aqueous interface could yield a lower-energy state. Although such a structural change could promote hydrophobic interactions with an oleate chain, it may also diminish the electrostatic forces helping to recruit the carboxylate out of water and into the protein cavity. Nonetheless, R122L/S124A LFABP can bind a single oleate without experiencing significant electrostatic perturbations (Figure 5D), much as reported for CRABP-(II) and IFABP (*44*−*46*). Like the double mutant, the potential surfaces for apo forms of CRABP(II) and IFABP lack positively charged residues like R122 or K90 facing the interior of the apoprotein cavity but have other positively charged groups capable of recruiting ionized fatty acid molecules; ILBP has a negatively charged interior and different ligand specificity (data not shown). Overall, our analysis suggests that although binding of oleate to FABPs should be accompanied by favorable entropic effects for expelled water molecules and is likely influenced by contrasting cavity sizes (*11*), the binding of multiple fatty acid molecules may also demand favorable protein−ligand energetics at each stage of the binding process.

Bound Oleate Environment in Diverse FABPs. It is well-established that despite the somewhat divergent primary sequences of the various FABPs, their tertiary structures exhibit a common clam-shell-like configuration, with two parallel β-sheets oriented orthogonally to each other to form a deep cavity in which hydrophobic ligands can be bound (*39*). The three-dimensional NMR-based structures of two oleate-bound FABP complexes have been reported: oleate-bound locust

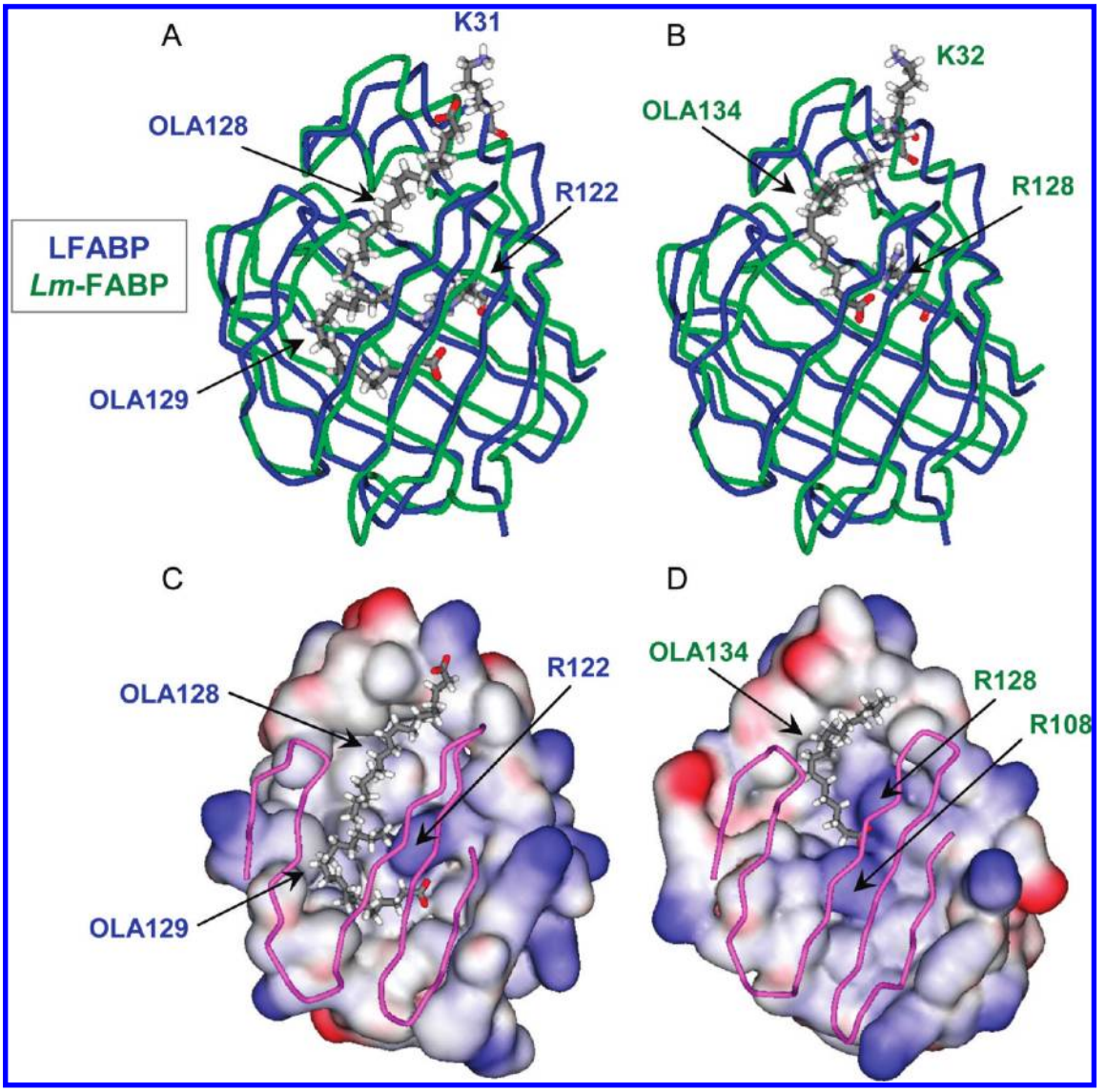

FIGURE 6: (A and B) Superposition with PDB Viewer for oleate-bound complex structures of LFABP (*8*) (blue) and locust muscle *Lm*-FABP (*4*) (green), displayed with DS ViewerPro. (A) Locations for the first oleate (OLA129) and the second oleate (OLA128) within LFABP. (B) Locations of the sole oleate (OLA134) within *Lm*-FABP. (C and D) Electrostatic potential surface views (same scheme as Figure 5) for LFABP (C) and *Lm*-FABP (D) complexes.

muscle *Lm*-FABP [133 residues, PDB entry 2flj (*4*)] and oleate-bound wild-type LFABP [127 residues, PDB entry 2ju8 (*8*)]. On the basis of the two superimposed backbone traces (Figure 6A,B), the $KR^{122}VS^{124}KR$ sequence in LFABP is aligned structurally with the $TR^{128}IY^{130}KA$ sequence in *Lm*-FABP. In both complexes, a hydrogen bond is formed from the carboxyl oxygen of the oleate ligand (OLA129 in LFABP and OLA134 in *Lm*-FABP) to an arginine side chain NH_2 group (R122 in LFABP and R128 in *Lm*-FABP), establishing a similar location and orientation for the respective oleate carboxyl groups. However, in the *Lm*-FABP−oleate complex, the formation of an additional hydrogen bond between the COO group of OLA134 and the side chain NH_2 group of R108 tethers the carboxyl head of OLA134 between R128 and R108, effectively preventing a repositioning to facilitate the entry of a second OLA ligand (Figure 6D). Additionally, the different sequences in the αII region ($IQK^{31}GKD$ in LFABP and $RK^{32}A^{33}GLA$ in *Lm*-FABP) produce slightly different lysine locations (K31 and K33 in LFABP and K32 in *Lm*-FABP) that could nevertheless account for different binding stoichiometries: two oleate ligands bind to LFABP, whereas only one oleate binds to *Lm*-FABP. As noted above, the OLA128 carboxyl of LFABP exhibits favorable electrostatic interactions with the ammonium side chain of K31 (Figure 6A). In *Lm*-FABP, however, the K31 side chain is replaced with the hydrophobic methyl group of A33.

CONCLUSIONS

By monitoring the stepwise titration of liver fatty acid-binding proteins using two-dimensional ^{15}N HSQC NMR, we were able to identify slowly exchanging structural variants that differ with respect to the number of bound ligands and associated conformational accommodations of the protein. These measurements revealed the number of bound fatty acids, the location of each ligand in the cavity of its protein binding partner, the sequence of binding sites that were occupied by successively entering ligands, and the protein structural adjustments associated with their respective entry; determining the structure of the macromolecular complex was not required. HSQC evidence of a protein:ligand stoichiometry of 1:2, with binding of the first oleate deep within

the cavity followed by the second fatty acid near the aqueous interface, was validated for wild-type LFABP by reference to published structural data (*8*, *14*). An analogous titration conducted for an R122L/S124A LFABP mutant revealed 1:1 stoichiometry and an intermediate ligand location within the protein cavity.

These contrasting modes of oleate binding for structurally similar FABPs (wild-type LFABP, R122L/S124A LFABP, and *Lm*-FABP) may be attributed to a variety of energetic and dynamic factors: both recruitment of the first oleate ligand and association with a second one appear to require favorable electrostatic interactions with positively charged amino acid side chains, whereas the capacity of a protein to bind two ligands is likely to rely upon both the cavity size and the facility for structural accommodations that promote hydrophobic interactions between the fatty acyl chains.

ACKNOWLEDGMENT

We thank Drs. Alan Kleinfeld and Ron Ogata for making available the rat LFABP cDNA. We gratefully acknowledge Drs. Marilyn Gunner, Junjun Mao, and Karin Hauser and Ms. Silmilly Toribio for conducting the MCCE calculations. We thank Dr. Judith Storch for valuable discussions and insights during the course of this project.

SUPPORTING INFORMATION AVAILABLE

Backbone HN chemical shifts (Tables S1 and S2) for wild-type and R122L/S124A LFABP at titration points of 1:0, 1:0.4, and 1:2. This material is available free of charge via the Internet at http://pubs.acs.org.

REFERENCES

1. Storch, J., and Thumser, A. E. (2000) The fatty acid transport function of fatty acid-binding proteins. *Biochim. Biophys. Acta 1486*, 28–44.
2. Storch, J., and Córsico, B. (2008) The emerging functions and mechanisms of mammalian fatty acid-binding proteins. *Annu. Rev. Nutr. 28*, 73–95.
3. Zimmerman, A. W., and Veerkamp, J. H. (2002) New insights into the structure and function of fatty acid-binding proteins. *Cell. Mol. Life Sci. 59*, 1096–1116.
4. Lucke, C., Qiao, Y., Van Moerkerk, H. T., Veerkamp, J. H., and Hamilton, J. A. (2006) Fatty-acid-binding protein from the flight muscle of *Locusta migratoria*: Evolutionary variations in fatty acid binding. *Biochemistry 45*, 6296–6305.
5. Banaszak, L., Winter, N., Xu, Z. H., Bernlohr, D. A., Cowan, S., and Jones, T. A. (1994) Lipid-binding proteins: A family of fatty-acid and retinoid transport proteins. *Adv. Protein Chem. 45*, 89–151.
6. Storch, J., and McDermott, L. (2009) Structural and functional analysis of fatty acid-binding proteins. *J. Lipid Res. 50* (Suppl.), S126–S131.
7. De Gerónimo, E., Hagan, R. M., Wilton, D. C., and Córsico, B. (2010) Natural ligand binding and transfer from liver fatty acid binding protein (LFABP) to membranes. *Biochim. Biophys. Acta 1801*, 1082–1089.
8. He, Y., Yang, X., Wang, H., Estephan, R., Francis, F., Kodukula, S., Storch, J., and Stark, R. E. (2007) Solution-state molecular structure of apo and oleate-liganded liver fatty acid-binding protein. *Biochemistry 46*, 12543–12556.
9. Nemecz, G., Jefferson, J. R., and Schroeder, F. (1991) Polyene fatty acid interactions with recombinant intestinal and liver fatty acid-binding proteins. *J. Biol. Chem. 266*, 17112–17123.
10. Cistola, D. P., Sacchettini, J. C., Banaszak, L. J., Walsh, M. T., and Gordon, J. I. (1989) Fatty acid interactions with rat intestinal and liver fatty acid-binding proteins expressed in *Escherichia coli*. *J. Biol. Chem. 264*, 2700–2710.
11. Thompson, J., Ory, J., Reese-Wagoner, A., and Banaszak, L. (1999) The liver fatty acid binding protein: Comparison of cavity properties of intracellular lipid-binding proteins. *Mol. Cell. Biochem. 192*, 9–16.
12. Sacchettini, J. C., Gordon, J. I., and Banaszak, L. (1989) Crystal structure of rat intestinal fatty-acid-binding protein: Refinement and analysis of the *Escherichia coli*-derived protein with bound palmitate. *J. Mol. Biol. 208*, 327–339.
13. Hsu, K. T., and Storch, J. (1996) Fatty acid transfer from liver and intestinal fatty acid-binding proteins to membranes occurs by different mechanisms. *J. Biol. Chem. 271*, 13317–13323.
14. Thompson, J., Winter, N., Terwey, D., Bratt, J., and Banaszak, L. (1997) The crystal structure of the liver fatty acid-binding protein. A complex with two bound oleates. *J. Biol. Chem. 272*, 7140–7150.
15. Borchers, T., and Spener, F. (1993) Involvement of arginine in the binding of heme and fatty acids to fatty acid-binding protein from bovine liver. *Mol. Cell. Biochem. 123*, 23–27.
16. Thumser, A. E., Evans, D., Worrall, A. F., and Wilton, D. C. (1994) Effect on ligand binding of arginine mutations in recombinant rat liver fatty acid-binding protein. *Biochem. J. 297*, 103–107.
17. Thumser, A. E., Voysey, J., and Wilton, D. C. (1996) Mutations of recombinant rat liver fatty acid-binding protein at residues 102 and 122 alter its structural integrity and affinity for physiological ligands. *Biochem. J. 314*, 943–949.
18. Wang, H., He, Y., Kroenke, C. D., Kodukula, S., Storch, J., Palmer, A. G., and Stark, R. E. (2002) Titration and exchange studies of liver fatty acid-binding protein with ^{13}C-labeled long-chain fatty acids. *Biochemistry 41*, 5453–5461.
19. Alexov, E. G., and Gunner, M. R. (1997) Incorporating protein conformational flexibility into the calculation of pH-dependent protein properties. *Biophys. J. 72*, 2075–2093.
20. Alexov, E. G., and Gunner, M. R. (1999) Calculated protein and proton motions coupled to electron transfer: Electron transfer from QA^- to QB in bacterial photosynthetic reaction centers. *Biochemistry 38*, 8253–8270.
21. Estephan, R. (2005) Effect of R122L/S124A and K31L mutations on molecular structure and function in rat liver fatty acid-binding protein. Ph.D. Dissertation, City University of New York, New York.
22. Richieri, G. V., Ogata, R. T., and Kleinfeld, A. M. (1994) Equilibrium constants for the binding of fatty acids with fatty acid-binding proteins from adipocyte, intestine, heart, and liver measured with fluorescent probe ADIFAB. *J. Biol. Chem. 269*, 23918–23930.
23. Hodsdon, M. E., and Cistola, D. P. (1997) Ligand binding alters the backbone mobility of intestinal fatty acid-binding protein as monitored by ^{15}N NMR relaxation and ^{1}H exchange. *Biochemistry 36*, 2278–2290.
24. Mittag, T., Franzoni, L., Cavazzini, D., Schaffhausen, B., Rossi, G. L., and Günther, U. (2006) Retinol modulates site-specific mobility of apo-cellular retinol-binding protein to promote ligand binding. *J. Am. Chem. Soc. 128*, 9844–9848.
25. Cogliati, C., Ragona, L., D'Onofrio, M., Günther, U., Whittaker, S., Ludwig, C., Tomaselli, S., Assfalg, M., and Molinari, H. (2010) *Chem.—Eur. J. 16*, 11300–11310.
26. Zhu, L., Kurian, E., Prendergast, F. G., and Kemple, M. D. (1999) Dynamics of palmitic acid complexed with rat intestinal fatty acid binding protein. *Biochemistry 38*, 1554–1561.
27. Dehner, A., Furrer, J., Richter, K., Schuster, I., Buchner, J., and Kessler, H. (2003) NMR chemical shift perturbation study of the N-terminal domain of Hsp90 upon binding of ADP, AMP-PNP, geldanamycin, and radicicol. *ChemBioChem 4*, 870–877.
28. McInnes, C., Grothe, S., O'Connor-McCourt, M., and Sykes, B. (2000) NMR study of the differential contributions of residues of transforming growth factor α to association with its receptor. *Protein Eng. 13*, 143–147.
29. Matter, H., Schudok, M., Elshorst, B., Jacobs, D., Saxena, K., and Kogler, H. (2005) QSAR-by-NMR: Quantitative insights into structural determinants for binding affinity by analysis of ^{1}H/^{15}N chemical shift differences in MMP-3 ligands. *Bioorg. Med. Chem. Lett. 15*, 1779–1783.
30. Shuker, S. B., Hajduk, P. J., Meadows, R. P., and Fesik, S. W. (1996) Discovering high-affinity ligands for proteins: SAR by NMR. *Science 274*, 1531–1534.
31. Salvatella, X., and Giralt, E. (2003) NMR-based methods and strategies for drug discovery. *Chem. Soc. Rev. 32*, 365–372.
32. Mulder, F. A. A., Schipper, D., Bott, R., and Boelens, R. (1999) Altered flexibility in the substrate-binding site of related native and engineered high-alkaline *Bacillus* subtilisins. *J. Mol. Biol. 292*, 111–123.
33. Medek, A., Hajduk, P. J., Mack, J., and Fesik, S. W. (2000) The use of differential chemical shifts for determining the binding site location and orientation of protein-bound ligands. *J. Am. Chem. Soc. 122*, 1241–1242.

34. Kay, L. E., Keifer, P., and Saarinen, T. (1992) Pure absorption gradient enhanced heteronuclear single quantum correlation spectroscopy with improved sensitivity. *J. Am. Chem. Soc. 114*, 10663–10665.
35. Wishart, D. S., and Sykes, B. D. (1994) The ^{13}C chemical-shift index: A simple method for the identification of protein secondary structure using ^{13}C-chemical shift data. *J. Biomol. NMR 4*, 171–180.
36. Delaglio, F., Grzesiek, S., Vuister, G. W., Zhu, G., Pfeifer, J., and Bax, A. (1995) NMRPipe: A multidimensional spectral processing system based on UNIX pipes. *J. Biomol. NMR 6*, 277–293.
37. Johnson, B. A., and Blevins, R. A. (1994) NMR View: A computer program for the visualization and analysis of NMR data. *J. Biomol. NMR 4*, 603–614.
38. Wang, H., He, Y., Hsu, K. T., Magliocca, J. F., Storch, J., and Stark, R. E. (1998) ^{1}H, ^{15}N and ^{13}C resonance assignments and secondary structure of apo liver fatty acid-binding protein. *J. Biomol. NMR 12*, 197–199.
39. Hamilton, J. (2004) Fatty acid interactions with proteins: What X-ray crystal and NMR solution structures tell us. *Prog. Lipid Res. 43*, 177–199.
40. Thompson, J., Reese-Wagoner, A., and Banaszak, L. (1999) Liver fatty acid binding protein: Species variation and the accommodation of different ligands. *Biochim. Biophys. Acta 1441*, 117–130.
41. Tochtrop, G. P., Richter, K., Tang, C., Toner, J. J., Covey, D. F., and Cistola, D. P. (2002) Energetics by NMR: Site-specific binding in a positively cooperative system. *Proc. Natl. Acad. Sci. U.S.A. 99*, 1847–1852.
42. Velkov, T., Chuang, S., Prankerd, R., Sakellaris, H., Porter, C. J. H., and Scanlon, M. J. (2005) An improved method for the purification of rat liver-type fatty acid binding protein from *Escherichia coli*. *Protein Expression Purif. 44*, 23–31.
43. Kim, J., Mao, J., and Gunner, M. R. (2005) Are acidic and basic groups in buried proteins predicted to be ionized? *J. Mol. Biol. 348*, 1283–1298.
44. Kurz, M., Brachvogel, V., Matter, H., Stengelin, S., Thuring, H., and Kramer, W. (2003) Insights into the bile acid transportation system: The human ileal lipid-binding protein-cholyltaurine complex and its comparison with homologous structures. *Proteins 50*, 312–328.
45. Wang, L., Li, Y., Abildgaard, F., Markley, J. L., and Yan, H. (1998) NMR solution structure of type II human cellular retinoic acid binding protein: Implications for ligand binding. *Biochemistry 37*, 12727–12736.
46. Hodsdon, M. E., and Cistola, D. P. (1997) Discrete backbone disorder in the nuclear magnetic resonance structure of apo intestinal fatty acid-binding protein: Implications for the mechanism of ligand entry. *Biochemistry 36*, 1450–1460.